

# Projected changes of the Northern Annular Mode linked to seasonality of the ENSO teleconnection

Takashi Kawamura<sup>1</sup>, Yu Kosaka<sup>2</sup>, Satoru Okajima<sup>1</sup>, and Hisashi Nakamura<sup>2</sup>

<sup>1</sup>Tokyo Daigaku Sentan Kagaku Gijutsu Kenkyu Center

<sup>2</sup>University of Tokyo

October 22, 2024

## Abstract

The Northern Annular Mode (NAM) is the dominant pattern of atmospheric circulation variability in the wintertime Northern Hemisphere extratropics. This study utilizes a large ensemble atmospheric simulation dataset to examine the seasonality of the NAM variability and its modulations under global warming. We show an enhancement of the Aleutian Low anomaly associated with the NAM in a warmer climate. This enhancement is related to the emergence of the Aleutian-Icelandic Low seesaw (AIS) from early winter, which is in contrast prominent only in late winter in the historical climate. The large ensemble reveals a significant increase in the fraction of the NAM variance explained by sea surface temperature and sea ice variability, suggesting a higher potential predictability. In particular, the eastward extension of the El Niño-Southern Oscillation (ENSO) teleconnection under global warming contributes to the AIS formation even in early winter and a higher NAM-ENSO correlation.

## Hosted file

Manuscript\_Kawamura\_etal2024\_GRL.docx available at <https://authorea.com/users/846334/articles/1234548-projected-changes-of-the-northern-annular-mode-linked-to-seasonality-of-the-ens-teleconnection>

1 **Projected changes of the Northern Annular Mode linked to seasonality of the ENSO**  
2 **teleconnection**

3  
4 **T. Kawamura<sup>1</sup>, Y. Kosaka<sup>1</sup>, S. Okajima<sup>1</sup>, and H. Nakamura<sup>1</sup>**

5 <sup>1</sup>Research Center for Advanced Science and Technology, the University of Tokyo, Japan

6  
7 Corresponding author: Takashi Kawamura ([tkawamura@atmos.rcast.u-tokyo.ac.jp](mailto:tkawamura@atmos.rcast.u-tokyo.ac.jp))

8  
9  
10 **Key Points:**

- 11 • The proportion of the Northern Annular Mode variance driven by variability of sea  
12 surface conditions increases in the warmer climate.
- 13 • This change is tied to early-winter emergence of the Aleutian-Icelandic Low seesaw  
14 which is limited to late winter in the present climate.
- 15 • Teleconnection from the El Niño-Southern Oscillation contributes to the earlier winter  
16 emergence of the seesaw in the warmer climate.  
17

## 18 **Abstract**

19 The Northern Annular Mode (NAM) is the dominant pattern of atmospheric circulation  
20 variability in the wintertime Northern Hemisphere extratropics. This study utilizes a large  
21 ensemble atmospheric simulation dataset to examine the seasonality of the NAM variability and  
22 its modulations under global warming. We show an enhancement of the Aleutian Low anomaly  
23 associated with the NAM in a warmer climate. This enhancement is related to the emergence of  
24 the Aleutian-Icelandic Low seesaw (AIS) from early winter, which is in contrast prominent only  
25 in late winter in the historical climate. The large ensemble reveals a significant increase in the  
26 fraction of the NAM variance explained by sea surface temperature and sea ice variability,  
27 suggesting a higher potential predictability. In particular, the eastward extension of the El Niño-  
28 Southern Oscillation (ENSO) teleconnection under global warming contributes to the AIS  
29 formation even in early winter and a higher NAM-ENSO correlation.

30

## 31 **Plain Language Summary**

32 Anomalous weather in the wintertime Northern Hemisphere extratropics is linked to the  
33 Northern Annular Mode (NAM). It manifests as the seesaw-like air pressure anomalies between  
34 the Arctic region and the midlatitude ocean basins. Despite its importance for climate risk  
35 assessment in a warming world, future changes in the year-to-year NAM variability have not  
36 been sufficiently investigated. Based on a large ensemble atmospheric simulation dataset of over  
37 10,000 model years, we show that the NAM in a warmer climate correlates more tightly with the  
38 El Niño-Southern Oscillation, a dominant climate mode over the tropical Pacific. Our finding  
39 suggests a higher potential predictability of the NAM under global warming.

40

## 41 **1 Introduction**

42 The Northern Annular Mode (NAM), also known as the Arctic Oscillation, is the most dominant  
43 pattern of atmospheric circulation variability in the wintertime Northern Hemisphere extratropics  
44 (Thompson & Wallace, 1998). The NAM features the same-signed sea-level pressure (SLP)  
45 anomalies around the climatological Aleutian Low (AL) and Azores High, and the opposite-  
46 signed SLP anomaly around the climatological Icelandic Low (IL). The two Atlantic lobes  
47 constitute the North Atlantic Oscillation (NAO), the dominant mode of variability in the North  
48 Atlantic. The NAM is also related to the strength of the polar vortex and represents a mode of  
49 variability extending from the troposphere to the stratosphere (Baldwin & Dunkerton, 1999;  
50 Kidston et al., 2015; Thompson & Wallace, 2000). Given the broad NAM influence on the  
51 surface climate (Thompson & Wallace, 1998; He et al., 2017; Thompson & Wallace, 2000),  
52 understanding its mechanisms is crucial for regional climate variability, extremes, and their  
53 seasonal forecasts.

54 Since identified by Thompson & Wallace (1998), the physical nature of the NAM has been  
55 debated. The main issue is its relationship with the NAO. The NAM spatially resembles the  
56 NAO in the North Atlantic sector, with a high temporal correlation between their indices.  
57 Wallace (2000) argued that the difference lies in whether one views the phenomenon locally  
58 (NAO) or hemispherically (NAM), as they are essentially the same. However, other studies  
59 questioned statistical (Deser 2000) and physical (Ambaum et al., 2001) linkages of the AL center

60 of action with the NAO. Among others, Honda & Nakamura (2001) discovered a prominent  
61 seesaw-like variability, named the Aleutian-Icelandic low seesaw (AIS), between the AL and IL  
62 during late winter. They suggested that the spatial pattern of the NAM is a result of the artificial  
63 mixing of the NAO and AIS through the empirical orthogonal function (EOF) analysis.

64 Climate model simulations suggest that the NAM shifts towards a more positive phase with  
65 global warming (Lee et al., 2021). However, aside from the mean state changes of the NAM,  
66 modulations of the statistical properties of NAM as an interannual variability remain to be  
67 elaborated further. In particular, its relationship with the AIS, which emerges in late winter in the  
68 present climate, as well as the spatial structure and amplitude of the NAM itself, have not been  
69 thoroughly investigated. In this study, we examine changes in these aspects under global  
70 warming using a large ensemble global atmospheric simulation dataset.

## 71 **2 Data and Methods**

### 72 **2.1 Data**

73 We use the database for Policy Decision making for Future climate change (d4PDF). d4PDF is a  
74 large ensemble of simulations by an atmospheric general circulation model (AGCM), MRI-  
75 AGCM3.2, with a 60 km horizontal resolution (Mizuta et al., 2017). The historical experiment  
76 (“HIST”) consists of 100-member ensemble simulations from 1951 to 2011, driven by observed  
77 sea surface temperatures (SST), sea ice, and external forcing factors such as greenhouse gases.  
78 d4PDF also includes a 90-member ensemble of global warming experiment (“+4K”), where the  
79 global mean surface temperature is increased to the 4°C global warming level. The SST imposed  
80 to +4K is derived by first removing the linear trend from the observations used for HIST, then  
81 adding climatological mean changes to match the global warming level. The spatial patterns of  
82 mean SST changes are derived from six selected models (Figure S1) of the Coupled Model  
83 Intercomparison Project Phase 5 (CMIP5; Taylor et al., 2012). The sea ice is also adjusted  
84 accordingly. The external forcing factors are based on the RCP8.5 scenario in the year 2090. For  
85 each of the six warming patterns, 15 ensemble simulations were conducted, comprising a 90-  
86 member ensemble of the +4K experiment. Note that interannual variability of SST is unchanged  
87 between HIST and +4K. All the data has been interpolated to 1.25-degree horizontal resolutions.

88 In d4PDF, small perturbations within the range of observational errors have been added to the  
89 prescribed SST, which differ among ensemble members. In this study, we disregard this  
90 influence and evaluate the variability of the ensemble mean as the component driven by SST and  
91 sea ice variability.

92 As a reference, we use the ERA5 reanalysis data (Hersbach et al., 2020) from 1940 to 2022 with  
93 a 1-degree horizontal resolution. Monthly SST data of COBE-SST2 (Hirahara et al., 2014),  
94 which served as the lower boundary condition for d4PDF, is also used for the period 1951-2011  
95 with a horizontal resolution of 1 degree.

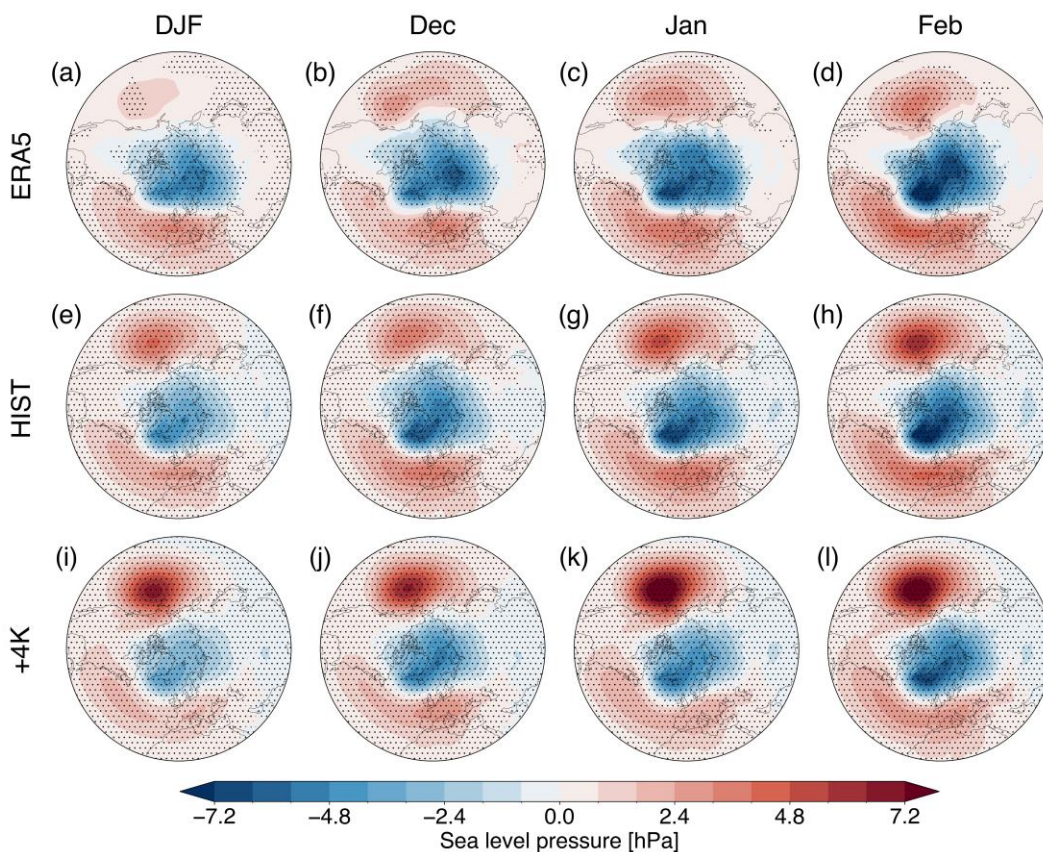
### 96 **2.3 Analysis methods**

97 Monthly climatology is calculated over the entire period (of the ensemble mean) of each  
98 dataset/experiment, and anomalies are defined as deviations from the monthly climatology. In

99 the +4K experiment, anomalies are defined relative to the climatology of individual warming  
 100 patterns. Following Thompson & Wallace (1998), an EOF analysis is performed on interannual  
 101 variability of monthly sea-level pressure (SLP) in the Northern Hemisphere extratropics (20-  
 102 90°N). This EOF analysis is applied separately to the December-February (DJF) average and  
 103 each calendar month from November to March. The NAM index is defined as the standardized  
 104 first principal component time series. For d4PDF HIST (+4K), unless noted otherwise, the NAM  
 105 index is defined for the variability over 6,000 (5,400) years, combining all ensemble members.  
 106 The statistical significance is tested using *t*-test, with the effective degree of freedom estimated  
 107 according to Bretherton et al. (1999).

### 108 3 Results

#### 109 3.1 Seasonality in the NAM and its change in a warmer climate



110

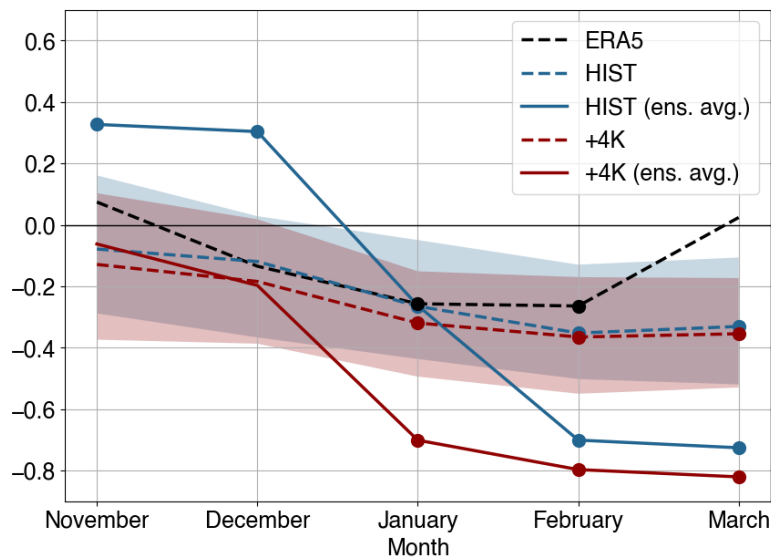
111 **Figure 1.** SLP anomalies (hPa) regressed onto the NAM index for (a) DJF-mean, (b) December,  
 112 (c) January, and (d) February based on ERA5 dataset. (e-h) and (i-l) are the same as (a-d), but for  
 113 d4PDF HIST and +4K, respectively. Dots indicate the statistical significance at the 95% level.

114 Figure 1 summarizes the SLP anomalies associated with the NAM. d4PDF reproduces the  
 115 overall structure and magnitude of the NAM reasonably well (Figure 1a-h). While d4PDF  
 116 overestimates the AL anomaly, as also found in a majority of CMIP5 (Gong et al., 2017; Zuo et  
 117 al., 2013) and CMIP6 (Coburn & Pryor, 2021) models, it successfully captures the observed

118 temporal correlations among three centers of action, namely the AL and two Atlantic lobes  
 119 (results not shown).

120 In both ERA5 and d4PDF HIST, the NAM exhibits an enhancement of the AL anomaly from  
 121 early to late winter. Indeed, the ratio of squared SLP anomaly over the AL region (40-55°N,  
 122 180°-150°W) to that of the North Atlantic sector (20-90°N, 90°W-40°E) increases from  
 123 December to February (1.3 times for ERA5 and 2.3 times for d4PDF). This result is qualitatively  
 124 unchanged against slight changes in the AL and North Atlantic domains.

125 In +4K, the NAM structure becomes more Pacific-weighted (Hamouda et al., 2021). Indeed,  
 126 while the SLP anomaly magnitudes at the Arctic and North Atlantic anomaly centers do not  
 127 change so much from the HIST experiment, the AL anomaly of the NAM in +4K strengthens  
 128 throughout winter (Figures 1i-l). As in HIST, the intensified AL anomaly also undergoes  
 129 intraseasonal strengthening from December to February.



130

131 **Figure 2.** Temporal correlation of SLP anomalies averaged over the AL (40-55°N, 180°-150°W)  
 132 and IL (60-70°N, 40-10°W) regions for each calendar month. Shading represents the 5th-95th  
 133 percentile range of d4PDF HIST (blue) and +4K (red) ensembles, with the median shown by a  
 134 dashed line. The black dashed line represents the correlation based on ERA5. Solid lines  
 135 represent the correlation between ensemble-averaged time series of HIST (blue) and +4K (red).  
 136 Dots indicate the statistical significance at the 95% level.

137 This seasonality of the NAM structure and its change under global warming are linked to the  
 138 AIS. Figure 2 shows the seasonality of the SLP anomaly correlation between the AL and IL  
 139 regions. In ERA5, the correlation is insignificant in November and December, but negatively  
 140 strengthens into late winter, becoming marginally significant in January and February (black  
 141 dashed line in Figure 2). This late-winter negative correlation represents the AIS (Honda &  
 142 Nakamura 2001). Since the AIS combined with the NAO can represent the NAM, the AIS  
 143 seasonality is consistent with the structural seasonality of the NAM.

144 Except for March, d4PDF HIST experiment captures the observed AIS within the ensemble  
 145 spread, demonstrating the capability of d4PDF to reproduce the NAM seasonality (blue shading  
 146 in Figure 2). The intraseasonal change of the correlation is more remarkable in the ensemble  
 147 mean (blue solid line in Figure 2), the component driven by the forcings external to the  
 148 atmosphere, namely SST and sea ice variability. In the HIST ensemble mean, the AL-IL  
 149 correlation is significantly positive in early winter (November and December), but turns  
 150 significantly negative in late winter (January and beyond).

151 In the +4K ensemble mean, the AL-IL correlation is more negative than in HIST throughout the  
 152 cold season, with a negative correlation already in December (red solid line in Figure 2). The  
 153 stronger negative correlation is also found in the all-member variability in +4K compared to  
 154 HIST in each calendar month (red shading in Figure 2). The disappearance of subseasonal  
 155 compensation and the strengthening of AL-IL correlation contribute to the structural changes of  
 156 the seasonally averaged NAM under global warming.

### 157 3.2 Externally forced component of the NAM

158 Next, we evaluate the externally (sea surface-) driven component of the NAM as the d4PDF  
 159 ensemble mean. The AL anomaly of the externally driven NAM strengthens from December to  
 160 February in both HIST and +4K (Figure S2). In December, the AL anomaly is almost missing in  
 161 HIST but obvious in +4K. This is consistent with the AIS emergence in early winter in the  
 162 warmer climate (Figure 2).

163 **Table 1.** Statistical properties of the NAM index. The ratio of the externally forced variance to  
 164 total variance of the NAM index (evaluated following Rowell et al., (1995)) and the correlation  
 165 between the ensemble-averaged NAM and the Niño 3.4 indices. Asterisks and daggers indicate  
 166 the 95% statistical significance of the non-zero correlations and their difference from those of  
 167 HIST, respectively.

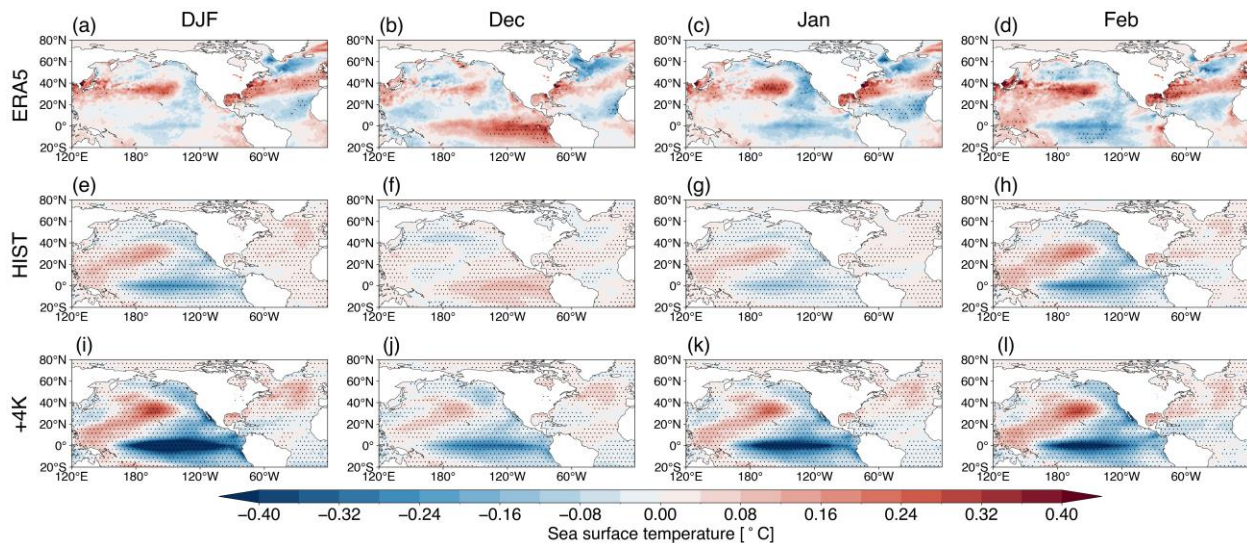
	Ratio of the ensemble-averaged NAM variance to the total variance				Correlation with the Niño 3.4 index			
	DJF	Dec	Jan	Feb	DJF	Dec	Jan	Feb
ERA5	-	-	-	-	-0.06	0.15	-0.12	-0.18
d4PDF HIST	9.5%	3.8%	4.8%	10.2%	-0.18*	0.06*	-0.09*	-0.24*
d4PDF +4K	31.0%	8.0%	17.3%	21.0%	-0.50* <sup>†</sup>	-0.21* <sup>†</sup>	-0.36* <sup>†</sup>	-0.41* <sup>†</sup>

168 Under global warming, the ratio of SST/sea ice-driven variance to total variance of the NAM  
 169 increases. In HIST, this ratio increases from early to late winter (d4PDF HIST of Table 1),  
 170 corresponding to the late winter emergence of the AIS. In +4K, this ratio more than doubles in  
 171 each calendar month compared with HIST (d4PDF +4K in Table 1). In the DJF mean, the ratio  
 172 increases more than threefold, since the intraseasonal compensation of the AL-IL correlation in  
 173 HIST disappears in +4K (Figure 2). These results suggest that the potential predictability of the

174 NAM increases under global warming. While the separate NAM definitions for HIST and +4K  
 175 might raise a concern of mixing up differences in spatial patterns and temporal behaviors, our  
 176 additional analyses with common spatial patterns confirm the robustness of the result (Table S1).

177 We also estimate the required ensemble size for robust signal detection. Following Mori et al.  
 178 (2014), we perform a bootstrap sampling from the ensembles of HIST and +4K and obtain the  
 179 NAM index from the subsampled members for the DJF mean variability (Figure S3). The 5th-  
 180 95th percentile range is well separated with 10 or more members. For individual calendar months,  
 181 50 and 20 or more members are required for December and February, respectively (Figures not  
 182 shown). It is noteworthy that our result is based on ensemble simulations of a single AGCM, and  
 183 thus the above members can be considered as the lower limits. The required ensemble size can  
 184 be even larger when the analysis is based on multi-model ensemble simulations.

### 185 3.3 ENSO teleconnection contributing to the seasonality

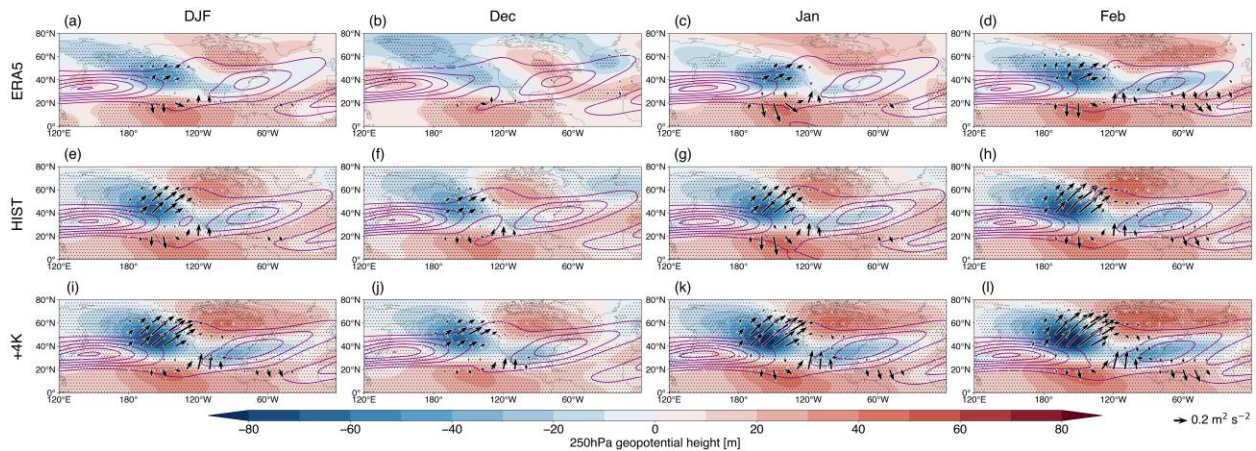


186

187 **Figure 3.** Same as Figure 1, but SST anomalies ( $^{\circ}\text{C}$ ) are regressed onto the NAM index.

188 We investigate the SST variability correlated with the NAM (Figure 3). In HIST, a distinct  
 189 polarity change in SST anomalies is evident over the equatorial Pacific from December to  
 190 February (Figures 3f-h), indicating that the positive NAM is associated with El Niño in  
 191 December but with La Niña in February. This intraseasonal reversal is also found based on the  
 192 NAO (Moron & Gouirand, 2003). In the warmer climate, in contrast, the polarity in December  
 193 changes, and the positive NAM is consistently associated with La Niña throughout winter. These  
 194 results suggest that the El Niño-Southern Oscillation (ENSO) is an important driver for the NAM  
 195 regarding both seasonality and changes under global warming.

196 Table 1 also shows the correlation of the NAM index with the Niño 3.4 index (the detrended SST  
 197 anomalies over the Niño 3.4 region, common to HIST and +4K). In HIST, the NAM-ENSO  
 198 correlation is positive and marginally significant in December and then transitions to significant  
 199 negative values in January and February, consistent with ERA5. In +4K, the correlation becomes  
 200 more negative, with a December value comparable to the HIST late-winter values. Again, these  
 201 results are robust against the different definitions of the NAM index (Table S1).



202

203 **Figure 4.** Z250 anomalies (shading, m) regressed onto the normalized Niño 3.4 index for (a)  
 204 DJF-mean, (b) December, (c) January, and (d) February based on ERA5. (e-h) and (i-l) are the  
 205 same as (a-d), but for d4PDF HIST and +4K, respectively. Arrows indicate the associated wave  
 206 activity flux ( $\text{m}^2 \text{s}^{-2}$ ; Takaya & Nakamura, 2001). Solid lines indicate climatological zonal wind  
 207 ( $5 \text{ m s}^{-1}$  interval from  $20 \text{ m s}^{-1}$ ). Dots indicate the statistical significance at the 95% level.

208 To understand the seasonality of the NAM-ENSO correlation and its changes under global  
 209 warming, we compare the ensemble-averaged 250 hPa geopotential height anomalies regressed  
 210 onto the Niño 3.4 index among ERA5, HIST, and +4K (Figure 4). A wavetrain pattern  
 211 emanating from the climatological jet exit over the Northeastern Pacific and extending eastward  
 212 through North America into the North Atlantic is evident in HIST, reproducing the observational  
 213 counterpart. In December of HIST, its downstream extension projects onto the positive NAO  
 214 over the North Atlantic, yielding the same-sign anomalies between the AL and IL. This is  
 215 consistent with the significant in-phase relationship between the two lows in December (blue  
 216 solid line in Figure 2) and the marginally significant positive correlation between NAM and  
 217 ENSO (Table 1). In February of HIST, by contrast, a meridional pair of positive and negative  
 218 anomalies extending eastward from North America into the Atlantic projects onto the negative  
 219 NAO, reflecting the seasonality of ENSO-NAO teleconnection (Abid et al., 2021; Geng et al.,  
 220 2023). Consequently, the AL and IL anomalies have the opposite sign, and the NAM-ENSO  
 221 correlation becomes negative.

222 In +4K, the meridional pair of the ENSO-related December height anomalies over North  
 223 America is stronger and elongated farther eastward than its HIST counterpart, resembling the  
 224 mid-to-late-winter pattern in HIST over North America and the North Atlantic (Figures 4g and  
 225 4j). This negative NAO-like pattern results in the AIS appearance even in early winter. This also  
 226 means a disappearance of the intraseasonal ENSO-NAO teleconnection reversal under global  
 227 warming, which is consistent with Geng et al. (2024). Furthermore, the negative NAM-ENSO  
 228 correlation in mid- to late winter strengthens. Consequently, there is a significant enhancement  
 229 of the negative NAM-ENSO correlation in the DJF average (Table 1).

## 230 4 Discussions

231 One of the possible mechanisms for the strengthening of the NAM-ENSO correlation is the  
 232 change in convective activity anomalies associated with ENSO under global warming (Power et

233 al., 2013; Yeh et al., 2018). In +4K, the ENSO convective anomalies are enhanced in the tropical  
234 Pacific, especially in its eastern portion, compared to HIST (Figure S4). The latter change acts to  
235 shift the ENSO-forced Rossby wavetrain eastward and better project onto the NAO in the  
236 opposite polarity with ENSO. This interpretation is consistent with previous studies (Drouard &  
237 Cassou, 2019; Kug et al., 2010). It should be noted that, since the structure and magnitude of  
238 ENSO's SST anomalies are the same between the HIST and +4K experiments, the change in  
239 atmospheric response is attributable to the background changes associated with global warming.

240 Besides, changes in the background jet stream due to global warming may affect the  
241 teleconnection of ENSO. Figure 4 suggests a Rossby wave propagation pathway from the Pacific  
242 midlatitude jet and another pathway from the subtropical Northeastern Pacific through Central  
243 America to the North Atlantic. The +4K experiment indicates that the westerly winds strengthen  
244 over the Northeastern Pacific and better connect the jets of the two ocean basins (Figure S5).  
245 This implies an enhanced propagation of Rossby waves from the Pacific to the Atlantic (Drouard  
246 & Cassou, 2019). A detailed investigation to verify this hypothesis is left for future work.

247 The above hypotheses depend on the spatial pattern of SST warming. For each of the six  
248 warming patterns imposed to +4K (Figure S1), we separately define the NAM index by the same  
249 procedure and evaluate the NAM-ENSO correlation. We focus on the pattern of equatorial  
250 Pacific warming, namely whether it is El Niño-like or not. Figure S6 examines the relationship  
251 between the climatological equatorial Pacific zonal SST gradient change and the correlation of  
252 the ensemble-averaged NAM with ENSO in December. Although the sample size is small, a  
253 negative inter-warming pattern correlation is clear, where the El Niño-like warming pattern tends  
254 to have a stronger NAM-ENSO correlation. The El Niño-like background SST warming causes  
255 the eastward shift of the ENSO convection anomalies (Bayr et al., 2014), letting the ENSO  
256 teleconnection reach farther eastward. Besides, El Niño-like SST warming leads to deepening the  
257 climatological AL and accelerating the Pacific jet stream (Gan et al., 2017), which can enhance  
258 the teleconnection toward the North Atlantic.

## 259 **5 Conclusions**

260 This study investigates the NAM seasonality and its modulations under global warming, using a  
261 large ensemble AGCM simulation dataset d4PDF. The HIST experiment confirms that the AL  
262 anomaly associated with NAM strengthens from early to late winter (Figures 1e-h). We show an  
263 enhanced AL anomaly throughout winter in a warmer climate (Figures 1i-l). This change is  
264 related to the seasonally earlier emergence and strengthening of the AIS (Figure 2). Our results  
265 demonstrate that the ENSO teleconnection reaches farther eastward with global warming and  
266 changes the AIS seasonality and strength (Figure 4, Table 1). The linkage between NAM and  
267 ENSO strengthens, leading to the increased proportion of NAM variance driven by SST and sea  
268 ice variability (Figure 3, Table 1).

269 The modulation in the NAM under global warming is similar to the change from early to late  
270 winter. In the historical climate, the NAM seasonality is affected by a contrasting ENSO-NAO  
271 teleconnection between early and late winter. Global warming leads to a seasonally consistent  
272 ENSO-NAO correlation, altering the NAM more like the late winter situation in the present  
273 climate.

274 It should be noted that this study benefits from the use of a single AGCM large ensemble. First,  
 275 the ensemble average represents the component driven by SST and sea ice variability. Evaluation  
 276 of the influence of sea surface condition variability on total NAM variance is thus  
 277 straightforward. Second, since SST variability is common between HIST and +4K, any change in  
 278 NAM variability is attributable to changes in the background condition. Yet, validation is  
 279 necessary to determine whether these results are robust in other models. In particular, it is worth  
 280 investigating whether the NAM changes identified in this study are common in other AGCMs  
 281 and whether they are robust against diverse changes in ENSO's SST anomalies in coupled  
 282 models.

### 283 **Acknowledgments**

284 The authors thank Mr. Kento Usui (The University of Tokyo) for his help in the initial stage of  
 285 this study. This work is supported by the Japan Ministry of Education, Culture, Sports, Science,  
 286 and Technology through the advanced studies of climate change projection (SENTAN: Grant  
 287 Number JPMXD0722680395) program, the Arctic Challenge for Sustainability II (ArCS II:  
 288 Grant Number JPMXD1420318865) Program, by the Japan Society for the Promotion of Science  
 289 through KAKENHI Grant Numbers JP19H05703, JP23K22570, JP23K25937, JP23K25946, and  
 290 JP24H02223, by the Environment Research and Technology Development Fund  
 291 (JPMEERF20242001) of the Environmental Restoration and Conservation Agency provided by  
 292 Ministry of the Environment of Japan, and by International Graduate Program for Excellence in  
 293 Earth-Space Science (IGPEES), a World-leading Innovative Graduate Study (WINGS) Program,  
 294 the University of Tokyo.

### 295 **Data Availability Statement**

296 The d4PDF dataset (Mizuta et al., 2017) used in this study is available through the Data  
 297 Integration and Analysis System Program (DIAS) repository (via  
 298 <https://diasjp.net/en/service/d4pdf-data-download/>). The ERA5 dataset (Hersbach et al., 2020)  
 299 used in this study is available online (via <https://doi.org/10.24381/cds.6860a573>). The COBE-  
 300 SST2 dataset (Hirahara et al., 2014) used in this study is available online (via  
 301 <https://psl.noaa.gov/data/gridded/data.cobe2.html>).

### 302 **References**

- 303 Abid, M. A., Kucharski, F., Molteni, F., Kang, I.-S., Tompkins, A. M., & Almazroui, M. (2021).  
 304 Separating the Indian and Pacific Ocean Impacts on the Euro-Atlantic Response to ENSO and Its  
 305 Transition from Early to Late Winter. *Journal of Climate*, *34*(4), 1531–1548.  
 306 <https://doi.org/10.1175/JCLI-D-20-0075.1>  
 307 Ambaum, M. H. P., Hoskins, B. J., & Stephenson, D. B. (2001). Arctic Oscillation or North  
 308 Atlantic Oscillation? *Journal of Climate*, *14*(16), 3495–3507. [https://doi.org/10.1175/1520-0442\(2001\)014<3495:AOONAO>2.0.CO;2](https://doi.org/10.1175/1520-0442(2001)014<3495:AOONAO>2.0.CO;2)  
 309 Baldwin, M. P., & Dunkerton, T. J. (1999). Propagation of the Arctic Oscillation from the  
 310 stratosphere to the troposphere. *Journal of Geophysical Research: Atmospheres*, *104*(D24),  
 311 30937–30946. <https://doi.org/10.1029/1999JD900445>  
 312 Bayr, T., Dommenges, D., Martin, T., & Power, S. B. (2014). The eastward shift of the Walker  
 313 Circulation in response to global warming and its relationship to ENSO variability. *Climate*  
 314 *Dynamics*, *43*(9), 2747–2763. <https://doi.org/10.1007/s00382-014-2091-y>  
 315

- 316 Bretherton, C. S., Widmann, M., Dymnikov, V. P., Wallace, J. M., & Bladé, I. (1999). The  
317 Effective Number of Spatial Degrees of Freedom of a Time-Varying Field. *Journal of Climate*,  
318 *12*(7), 1990–2009. [https://doi.org/10.1175/1520-0442\(1999\)012<1990:TENOSD>2.0.CO;2](https://doi.org/10.1175/1520-0442(1999)012<1990:TENOSD>2.0.CO;2)
- 319 Coburn, J., & Pryor, S. C. (2021). Differential Credibility of Climate Modes in CMIP6. *Journal*  
320 *of Climate*, *34*(20), 8145–8164. <https://doi.org/10.1175/JCLI-D-21-0359.1>
- 321 Deser, C. (2000). On the teleconnectivity of the “Arctic Oscillation.” *Geophysical Research*  
322 *Letters*, *27*(6), 779–782. <https://doi.org/10.1029/1999GL010945>
- 323 Drouard, M., & Cassou, C. (2019). A Modeling- and Process-Oriented Study to Investigate the  
324 Projected Change of ENSO-Forced Wintertime Teleconnectivity in a Warmer World. *Journal of*  
325 *Climate*, *32*(23), 8047–8068. <https://doi.org/10.1175/JCLI-D-18-0803.1>
- 326 Gan, B., Wu, L., Jia, F., Li, S., Cai, W., Nakamura, H., et al. (2017). On the Response of the  
327 Aleutian Low to Greenhouse Warming. *Journal of Climate*, *30*(10), 3907–3925.  
328 <https://doi.org/10.1175/JCLI-D-15-0789.1>
- 329 Geng, X., Zhao, J., & Kug, J.-S. (2023). ENSO-driven abrupt phase shift in North Atlantic  
330 oscillation in early January. *Npj Climate and Atmospheric Science*, *6*(1), 1–8.  
331 <https://doi.org/10.1038/s41612-023-00414-2>
- 332 Geng, X., Kug, J.-S., & Kosaka, Y. (2024). Future changes in the wintertime ENSO-NAO  
333 teleconnection under greenhouse warming. *Npj Climate and Atmospheric Science*, *7*(1), 1–12.  
334 <https://doi.org/10.1038/s41612-024-00627-z>
- 335 Gong, H., Wang, L., Chen, W., Chen, X., & Nath, D. (2017). Biases of the wintertime Arctic  
336 Oscillation in CMIP5 models. *Environmental Research Letters*, *12*(1), 014001.  
337 <https://doi.org/10.1088/1748-9326/12/1/014001>
- 338 Hamouda, M. E., Pasquero, C., & Tziperman, E. (2021). Decoupling of the Arctic Oscillation  
339 and North Atlantic Oscillation in a warmer climate. *Nature Climate Change*, *11*(2), 137–142.  
340 <https://doi.org/10.1038/s41558-020-00966-8>
- 341 He, S., Gao, Y., Li, F., Wang, H., & He, Y. (2017). Impact of Arctic Oscillation on the East  
342 Asian climate: A review. *Earth-Science Reviews*, *164*, 48–62.  
343 <https://doi.org/10.1016/j.earscirev.2016.10.014>
- 344 Hersbach, H., Bell, B., Berrisford, P., Hirahara, S., Horányi, A., Muñoz-Sabater, J., et al. (2020).  
345 The ERA5 global reanalysis. *Quarterly Journal of the Royal Meteorological Society*, *146*(730),  
346 1999–2049. <https://doi.org/10.1002/qj.3803>
- 347 Hirahara, S., Ishii, M., & Fukuda, Y. (2014). Centennial-Scale Sea Surface Temperature  
348 Analysis and Its Uncertainty. *Journal of Climate*, *27*(1), 57–75. <https://doi.org/10.1175/JCLI-D-12-00837.1>
- 349
- 350 Honda, M., & Nakamura, H. (2001). Interannual Seesaw between the Aleutian and Icelandic  
351 Lows. Part II: Its Significance in the Interannual Variability over the Wintertime Northern  
352 Hemisphere. *Journal of Climate*, *14*(24), 4512–4529. [https://doi.org/10.1175/1520-0442\(2001\)014<4512:ISBTAA>2.0.CO;2](https://doi.org/10.1175/1520-0442(2001)014<4512:ISBTAA>2.0.CO;2)
- 353
- 354 Kidston, J., Scaife, A. A., Hardiman, S. C., Mitchell, D. M., Butchart, N., Baldwin, M. P., &  
355 Gray, L. J. (2015). Stratospheric influence on tropospheric jet streams, storm tracks and surface  
356 weather. *Nature Geoscience*, *8*(6), 433–440. <https://doi.org/10.1038/ngeo2424>
- 357 Kug, J.-S., An, S.-I., Ham, Y.-G., & Kang, I.-S. (2010). Changes in El Niño and La Niña  
358 teleconnections over North Pacific–America in the global warming simulations. *Theoretical and*  
359 *Applied Climatology*, *100*(3), 275–282. <https://doi.org/10.1007/s00704-009-0183-0>
- 360 Lee, J.-Y., Marotzke, J., Bala, G., Cao, L., Corti, S., Dunne, J. P., et al. (2021). Future global  
361 climate: scenario-based projections and near-term information. In V. Masson-Delmotte, P. Zhai,

- 362 A. Pirani, S. L. Connors, C. Péan, S. Berger, et al. (Eds.), *Climate Change 2021: The Physical*  
363 *Science Basis. Contribution of Working Group I to the Sixth Assessment Report of the*  
364 *Intergovernmental Panel on Climate Change* (pp. 553–672). Cambridge, United Kingdom and  
365 New York, NY, USA: Cambridge University Press. <https://doi.org/10.1017/9781009157896.001>
- 366 Mizuta, R., Murata, A., Ishii, M., Shiogama, H., Hibino, K., Mori, N., et al. (2017). Over 5,000  
367 Years of Ensemble Future Climate Simulations by 60-km Global and 20-km Regional  
368 Atmospheric Models. *Bulletin of the American Meteorological Society*, 98(7), 1383–1398.  
369 <https://doi.org/10.1175/BAMS-D-16-0099.1>
- 370 Mori, M., Watanabe, M., Shiogama, H., Inoue, J., & Kimoto, M. (2014). Robust Arctic sea-ice  
371 influence on the frequent Eurasian cold winters in past decades. *Nature Geoscience*, 7(12), 869–  
372 873. <https://doi.org/10.1038/ngeo2277>
- 373 Moron, V., & Gouirand, I. (2003). Seasonal modulation of the El Niño–southern oscillation  
374 relationship with sea level pressure anomalies over the North Atlantic in October–March 1873–  
375 1996. *International Journal of Climatology*, 23(2), 143–155. <https://doi.org/10.1002/joc.868>
- 376 Power, S., Delage, F., Chung, C., Kociuba, G., & Keay, K. (2013). Robust twenty-first-century  
377 projections of El Niño and related precipitation variability. *Nature*, 502(7472), 541–545.  
378 <https://doi.org/10.1038/nature12580>
- 379 Rowell, D. P., Folland, C. K., Maskell, K., & Ward, M. N. (1995). Variability of summer rainfall  
380 over tropical north Africa (1906–92): Observations and modelling. *Quarterly Journal of the*  
381 *Royal Meteorological Society*, 121(523), 669–704. <https://doi.org/10.1002/qj.49712152311>
- 382 Takaya, K., & Nakamura, H. (2001). A Formulation of a Phase-Independent Wave-Activity Flux  
383 for Stationary and Migratory Quasigeostrophic Eddies on a Zonally Varying Basic Flow. *Journal*  
384 *of the Atmospheric Sciences*, 58(6), 608–627. [https://doi.org/10.1175/1520-0469\(2001\)058<0608:AFOAPI>2.0.CO;2](https://doi.org/10.1175/1520-0469(2001)058<0608:AFOAPI>2.0.CO;2)
- 386 Taylor, K. E., Stouffer, R. J., & Meehl, G. A. (2012). An Overview of CMIP5 and the  
387 Experiment Design. *Bulletin of the American Meteorological Society*, 93(4), 485–498.  
388 <https://doi.org/10.1175/BAMS-D-11-00094.1>
- 389 Thompson, D. W. J., & Wallace, J. M. (1998). The Arctic oscillation signature in the wintertime  
390 geopotential height and temperature fields. *Geophysical Research Letters*, 25(9), 1297–1300.  
391 <https://doi.org/10.1029/98GL00950>
- 392 Thompson, D. W. J., & Wallace, J. M. (2000). Annular modes in the extratropical circulation.  
393 Part I: Month-to-month variability. *Journal of Climate*, 13(5), 1000–1016.
- 394 Wallace, J. M. (2000). North atlantic oscillationannular mode: Two paradigms—one  
395 phenomenon. *Quarterly Journal of the Royal Meteorological Society*, 126(564), 791–805.  
396 <https://doi.org/10.1002/qj.49712656402>
- 397 Yeh, S.-W., Cai, W., Min, S.-K., McPhaden, M. J., Dommenges, D., Dewitte, B., et al. (2018).  
398 ENSO Atmospheric Teleconnections and Their Response to Greenhouse Gas Forcing. *Reviews*  
399 *of Geophysics*, 56(1), 185–206. <https://doi.org/10.1002/2017RG000568>
- 400 Zuo, J.-Q., Li, W.-J., & Ren, H.-L. (2013). Representation of the Arctic Oscillation in the CMIP5  
401 Models. *Advances in Climate Change Research*, 4(4), 242–249.  
402 <https://doi.org/10.3724/SP.J.1248.2013.242>

*Geophysical Research Letters*

Supporting Information for

**“Projected changes of the Northern Annular Mode linked to seasonality of the ENSO teleconnection”**

T. Kawamura<sup>1</sup>, Y. Kosaka<sup>1</sup>, S. Okajima<sup>1</sup>, and H. Nakamura<sup>1</sup>

<sup>1</sup>Research Center for Advanced Science and Technology, the University of Tokyo, Japan

**Contents of this file**

Figures S1 to S6

Table S1

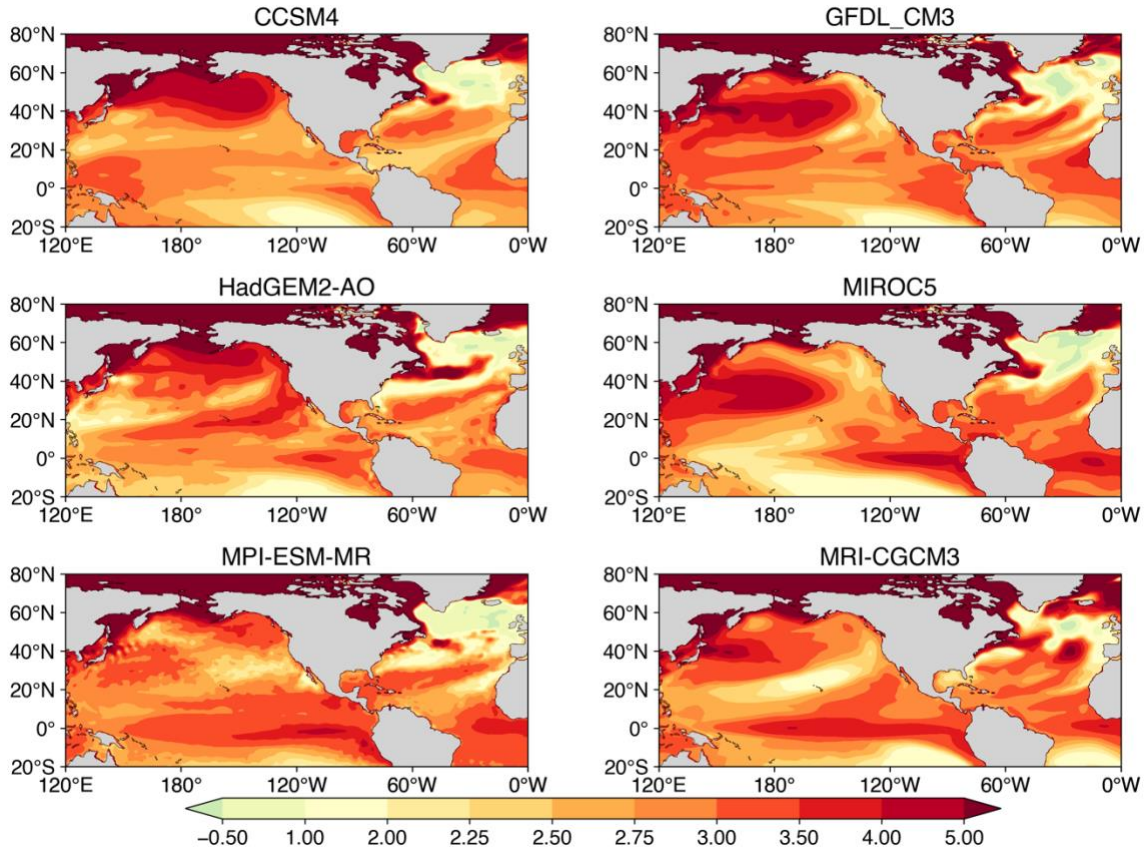


**Figure S1.** SST change pattern (°C) prescribed to d4PDF +4K experiment for each CMIP5 coupled model. November to March (NDJFM) averages are shown.

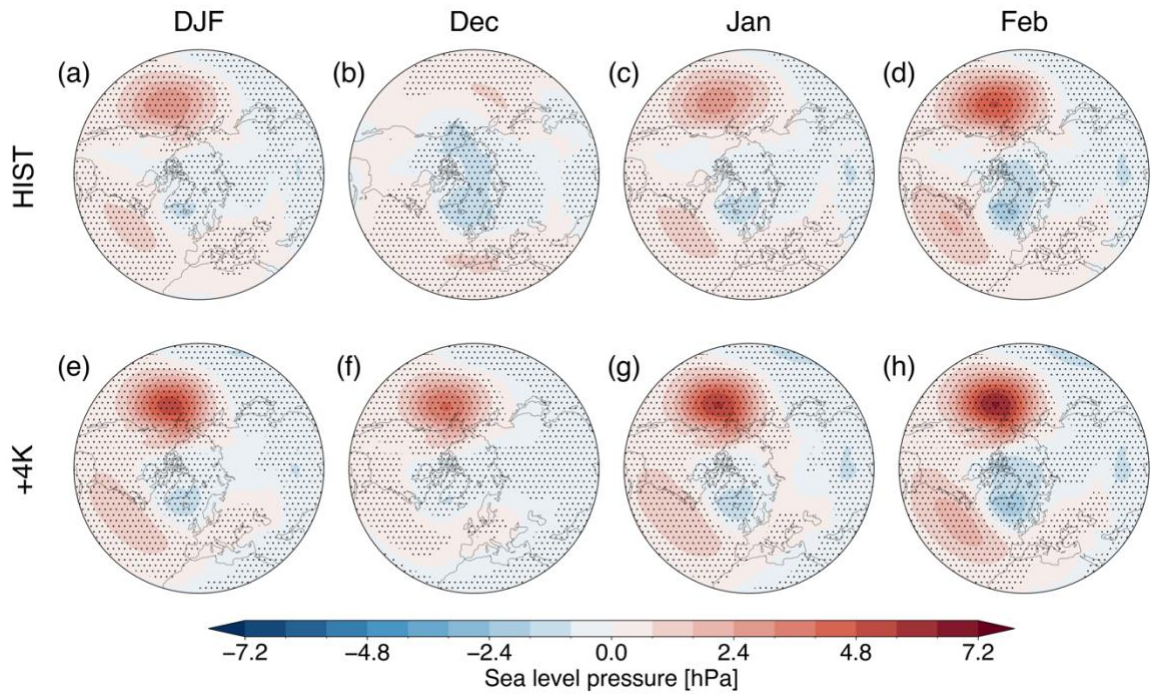


**Figure S2.** Same as the middle and bottom panels of Figure 1, but for the ensemble averaged SLP anomalies (hPa) regressed onto the ensemble averaged NAM index.

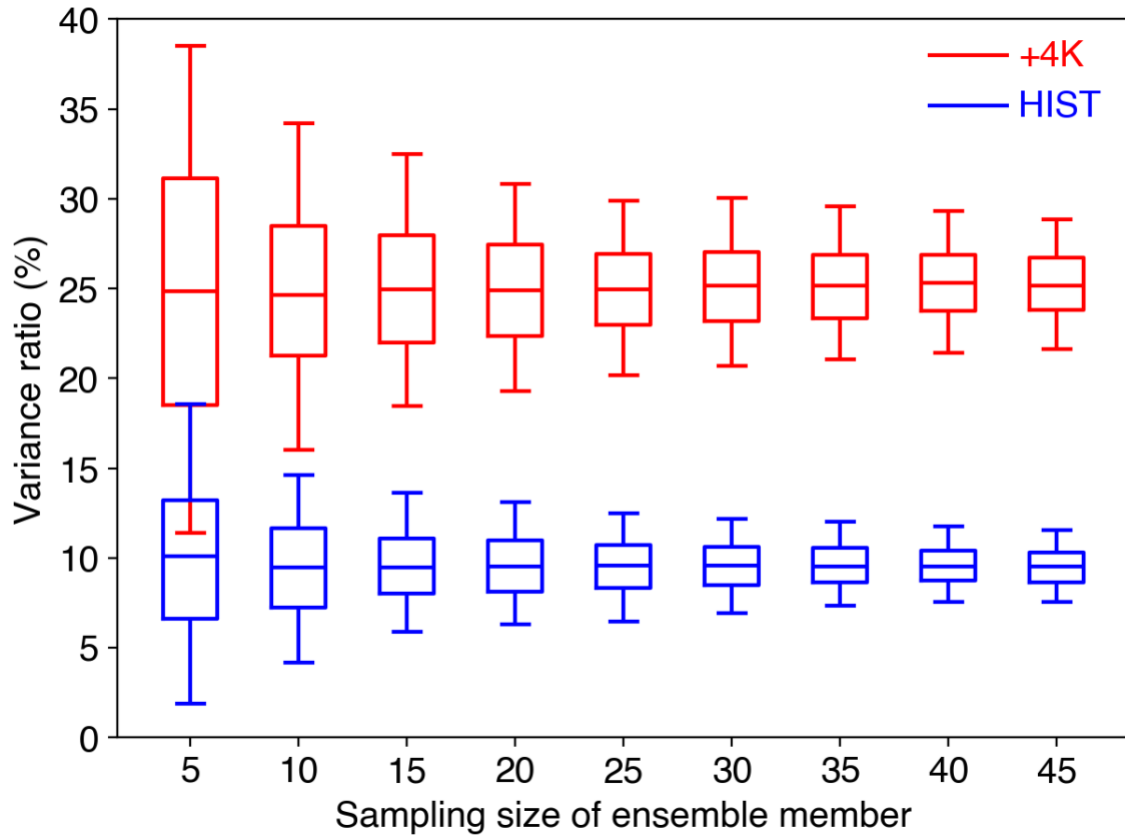


**Figure S3.** Box-and-whisker plots of the ratio of the variance of the externally forced component of the NAM index for DJF-mean as a function of subsampled ensemble size. Boxes and whiskers indicate ranges of one standard deviation and the 5th/95th percentile, respectively. Estimations are based on bootstrap random sampling (1,000 times). An EOF analysis is conducted on subsampled ensemble members.

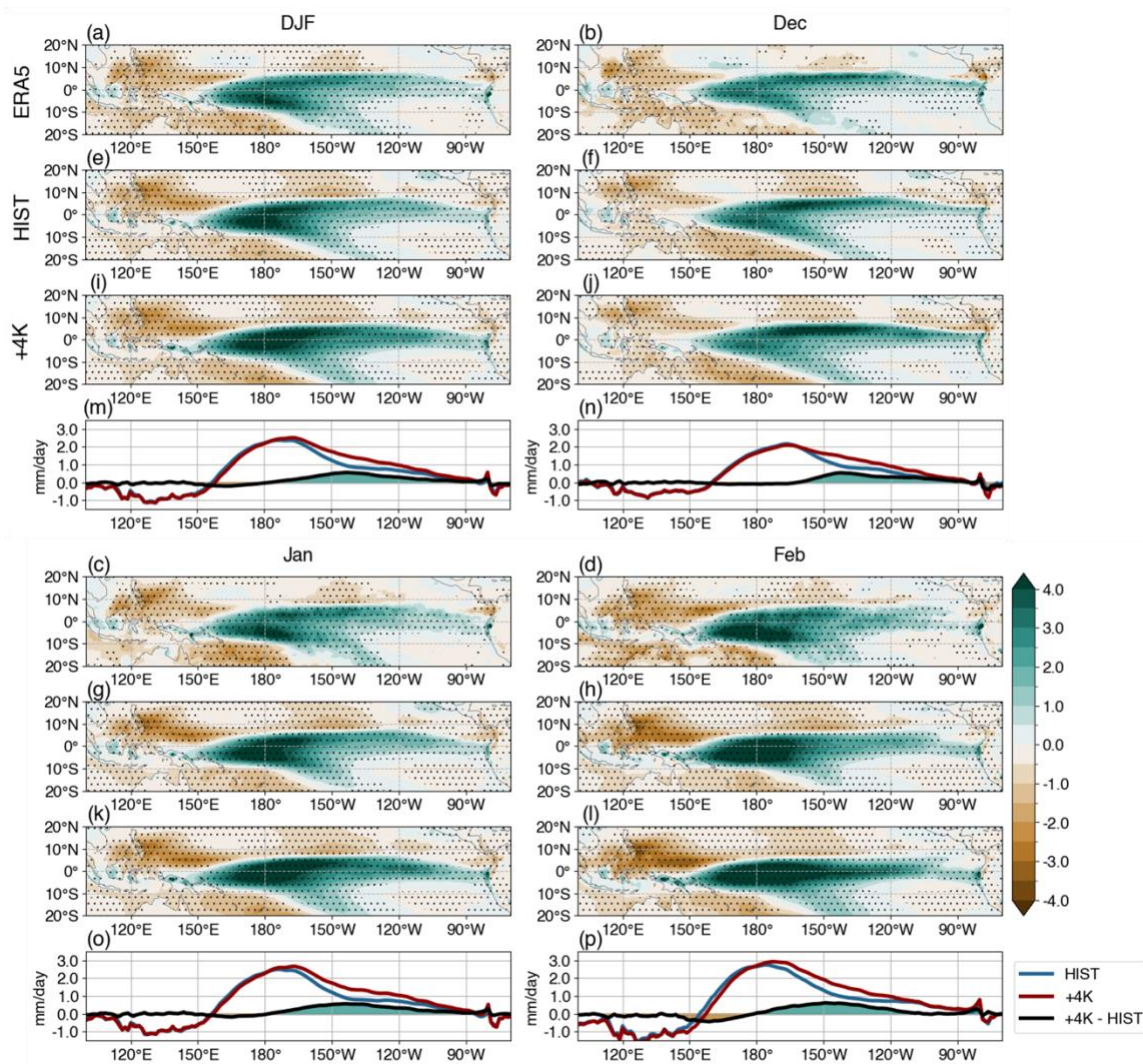


**Figure S4.** (a-l) Same for Figure 4, but for precipitation anomalies (mm/day) regressed onto the normalized Niño 3.4 index. (m-p) Zonal section of meridional averaged precipitation anomalies for d4PDF HIST (blue lines) and +4K (red lines) and their difference (black lines and shadings) over 10°S-10°N.

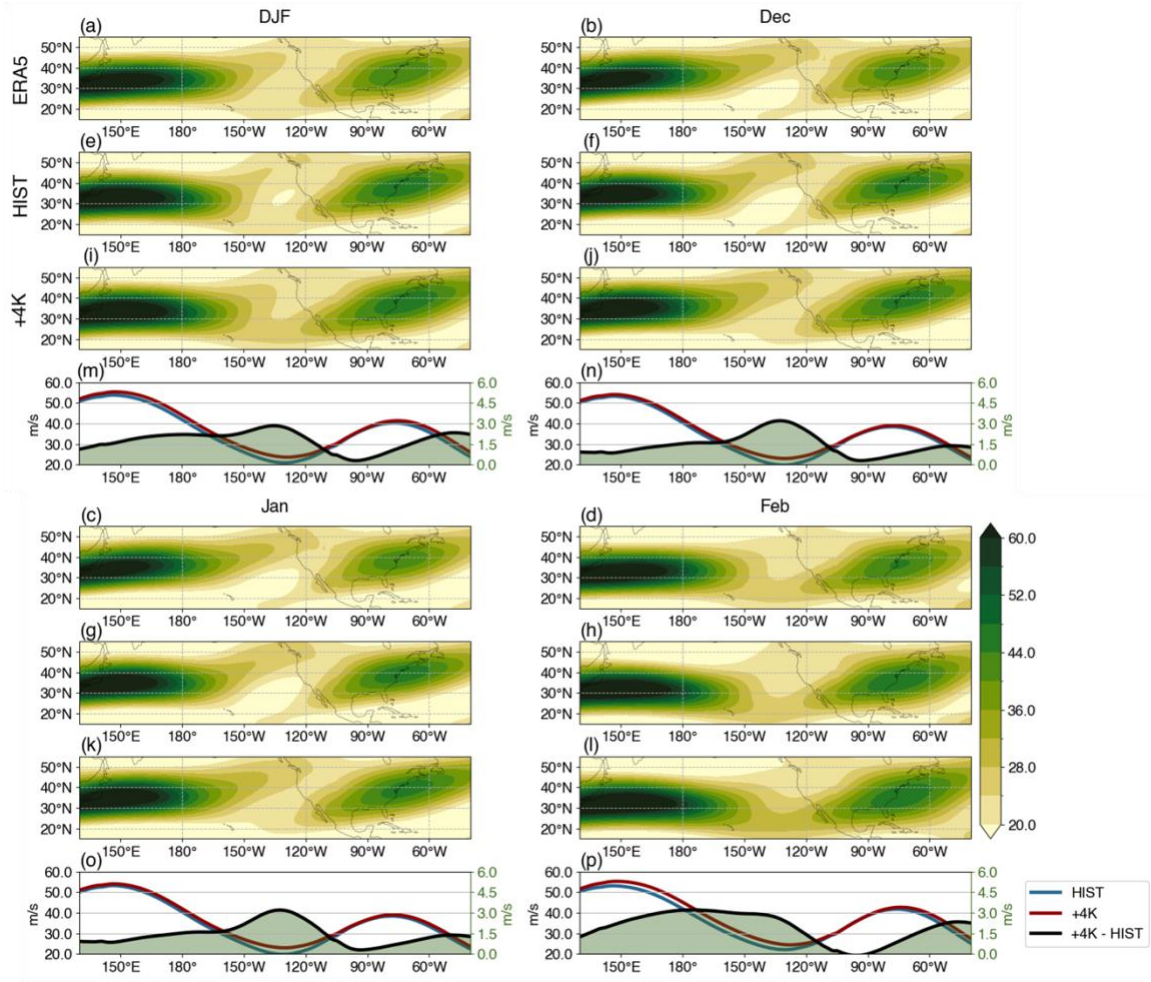


**Figure S5.** (a-l) Climatological zonal wind (m/s) at 250 hPa height for (a) DJF-mean, (b) December, (c) January, and (d) February based on the ERA5 dataset. (e-h) and (i-l) are the same as (a-d), but for d4PDF HIST and +4K, respectively. (m-p) Zonal section of meridional averaged zonal wind for d4PDF HIST (blue lines) and +4K (red lines) and their difference (black lines and shadings) over 25°-45°N for (m) DJF-mean, (n) December, (o) January, and (p) February.

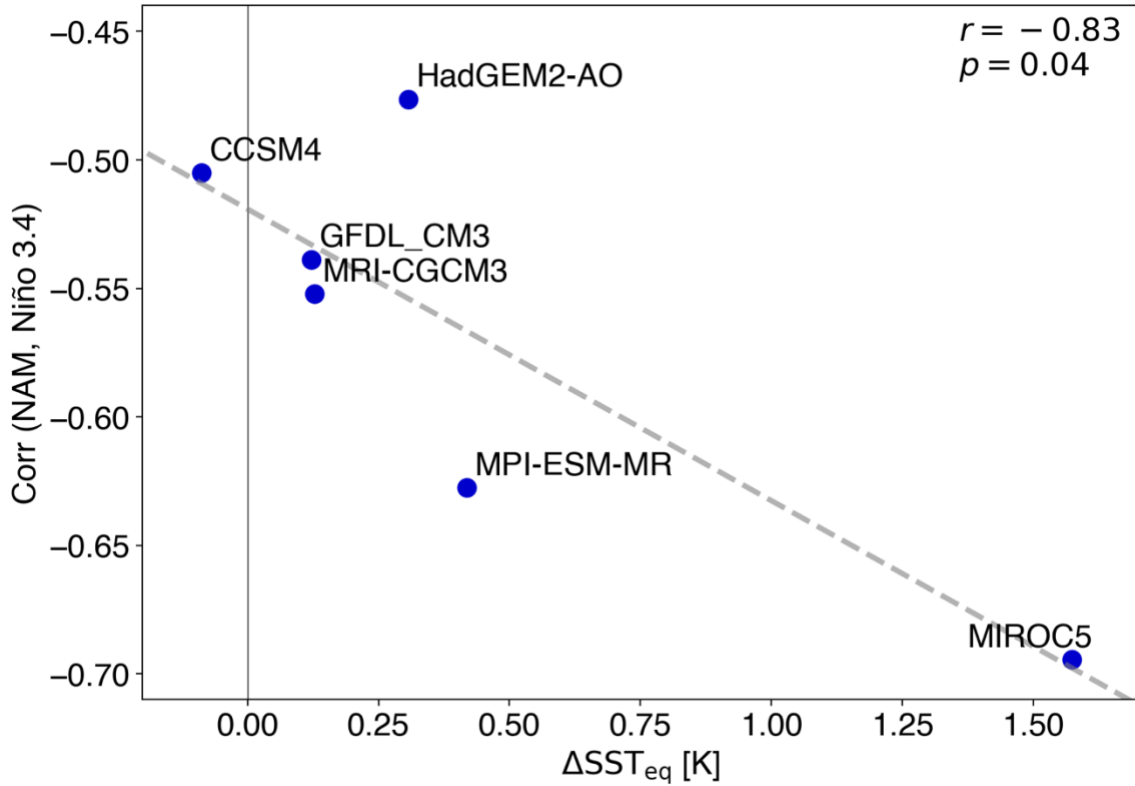


**Figure S6.** A scatterplot showing the correlation of the ensemble-averaged NAM index with the Niño 3.4 index in December of d4PDF +4K against climatological zonal SST gradient change in the equatorial Pacific. The latter is measured as the difference in SST changes between the eastern (5°S-5°N, 80°-130°W) and western (5°S-5°N, 150°E-160°W) equatorial Pacific. The NAM-Niño 3.4 correlation is calculated from the NAM index defined for each 15-member ensemble of a given SST change pattern. A dashed line indicates the linear fitting. The inter-warming pattern correlation ( $r$ ) and corresponding  $p$ -value are shown at the top right.

**Table S1.** Same as Table 1, but based on different definitions of the NAM index. Concatenated: an EOF analysis is conducted across the two experiments (HIST and +4K) of d4PDF, that is, an 11,400-year anomaly time series is used. Fixed to HIST: the index of +4K is defined as the projection time series onto the EOF1 pattern based on HIST. Ensemble mean: an EOF analysis is conducted on the ensemble-averaged anomalies.

		Ratio of the ensemble-averaged NAM variance to the total variance				Correlation with the Niño 3.4 index			
		DJF	Dec	Jan	Feb	DJF	Dec	Jan	Feb
d4PDF HIST	Concatenated	12.0%	3.5%	5.8%	10.9%	-0.24*	0.03*	-0.12*	-0.25*
	Ensemble mean	-	-	-	-	-0.90*	-0.86*	-0.86*	-0.87*
d4PDF +4K	Concatenated	20.2%	3.3%	9.6%	15.4%	-0.39*†	-0.10*†	-0.25*†	-0.34*†
	Fixed to HIST	16.8%	2.7%	7.9%	14.9%	-0.39*†	-0.09*†	-0.26*†	-0.38*†
	Ensemble mean	-	-	-	-	-0.94*	-0.85*	-0.91*	-0.92*